Nodal Admittance Matrix Based Area Partition Method for Small-Signal Stability Analysis of Large-Scale Power Electronics Based Power Systems

Liang Qiao [1], Yaosuo Xue[2], Le Kong[1], Fred Wang[1, 2]

[1] Center for Ultra-wide-area Resilient Electric Energy Transmission Networks (CURENT),
The University of Tennessee, Knoxville, TN, USA

[2]Oak Ridge National Laboratory, Oak Ridge, TN, USA

lqiao1@vols.utk.edu

***Abstract*—In power electronics-based power systems (PEPSs), small-signal stability is an important factor for system design and operation, where the impedance-based approach is often used. However, unlike small-scale PEPSs with simple and straightforward impedance models, it would take much more efforts to derive the large-scale PEPSs impedance model, which is very complicated and sometimes may get wrong results due to the elimination of right-half plane (RHP) poles during the impedance aggregation process. To simplify the derivation procedure and analyze the small-signal stability of large-scale PEPSs, this paper proposes a nodal admittance matrix (NAM) based area partition method. In this method, the large-scale PEPS is divided into several sub-areas, and the stability is analyzed within the sub-area first, and then the interconnection stability among these sub-areas is analyzed. The proposed method is scalable and can help to locate the weakest areas/converters that may cause instability in the whole system. In this paper, the concept of the proposed method and its application to an example system are introduced. Experimental results are also given to validate the effectiveness of the proposed method.**

Keywords—small-signal stability, nodal admittance matrix, area partition, power electronics-based power systems, large-scale

I. INTRODUCTION

Modern power systems are integrating more and more renewable generations and modern power-electronics interfaced loads, which lead to the increasing penetration level of power electronics converters [1-3]. In power electronics-based power systems, small-signal stability issues across a wide frequency range due to the impedance interactions among converters are concerned. Especially when it comes to large-scale PEPSs, practical methods to predict the system's small-signal stability are needed [4]. Typically, there are two types of approaches to analyze the small-signal stability of PEPSs [5]: the state-space model and the impedance model. The state-space approach requires detailed information of all system components. The impedance-based approach, on the other hand, uses terminal characteristics to analyze the stability, and does not require detailed internal control and system information of the converters. Thus, the impedance-based approach is adopted here for the small-signal stability analysis of large-scale PEPSs.

When using impedance-based approaches to analyze small-signal stability, there are mainly three types of criteria [6]: the generalized Nyquist criterion (GNC)-based, the loop impedance model (LIM)-based, and the Nodal admittance matrix (NAM)-based criteria. The GNC-based criterion is sensitive to the partition points, which may result in contradictory analysis results [7]. Also, both GNC-based and LIM-based criteria may have the pole-zero cancellation issue when performing the impedance aggregation [8] and thus would lead to inaccurate prediction results. The NAM-based criterion, on the contrary, preserves the system structure by using the admittance matrix and thus having fewer restrictions compared to the other two criteria. Therefore, the NAM-based criterion is preferred for the small-signal stability prediction of large-scale systems. However, in the existing works, when applying the NAM-based criterion, the admittance matrix is normally directly derived for the entire system [6, 9, 10]. It is not easy to be applied with the increasing system size since the dimension of the matrices is related to the number of converters in the system. The larger the system is, the larger and more complex the impedance matrix will be. Moreover, if the contingencies are considered, e.g., disconnection of some converters, the whole impedance matrix will need to be derived again from scratch.

Therefore, in this paper, an area partition method in combination with the NAM criterion is proposed for the small-signal stability analysis of large-scale PEPSs. By decomposing the large system into several sub-areas and their interconnection network, the proposed method can: 1) improve the scalability of the NAM criterion and save efforts on deriving impedance matrices when the contingency is considered; 2) provide more information about relatively independent subareas and their interconnection; 3) help to identify the areas/converters that mainly related to system instability in large-scale systems.

The rest of this paper is organized as follows. Section II explains the concept of the proposed NAM-based area partition method. In section III, the stability analysis of an example system is presented using the proposed method under different scenarios, together with the simulation results. Section IV provides the experimental results of the example system. Conclusions and future work are summarized in section V.

II. Concept of The Proposed NAM-Based Area Partition Method

A. Review of the Whole System NAM Method

When applying the NAM-based criteria for the whole system, a PEPS can be decomposed into individual converters and the passive connection network based on the component connection method (CCM) [9]. The overall system model is regarded as an equivalent multi-input multi-output (MIMO) negative feedback system. The closed-loop disturbance-to-output transfer function matrix $G_{cd}(s)$, is a diagonal matrix composed with output impedance or admittance of each converter in the system. The impedance matrix model of the connection network $G_{nw}(s)$, which also represents the output-to-disturbance transfer function matrix, can be derived based on the connection network. Since all converters are designed to be stable individually, the system stability can then be predicted using the determinant of the return-difference matrix $F(s)$:

$$F(s) = I + G_{cd}(s)G_{nw}(s) \tag{1}$$

The system is stable if and only if $N_{(0,j0)}(\det(F))$ is 0. In this method, the admittance matrices are derived directly for the whole system. Therefore, the dimensions of these matrices are directly related to the number of converters in the system. They will be very large matrices when applying the method to a very large PEPS with a large number of converters. Moreover, the stability of relatively independent sub-areas and their interactions are unclear with the single admittance matrix of the whole system.

B. The Proposed NAM-Based Area Partition Method

In the proposed method, a large-scale system is decomposed into m sub-areas and the corresponding interconnection network, as shown in Fig. 1, where each sub-area contains individual converters and their connection network. Fig. 2 shows the flow chart of the proposed method. The detailed steps of the proposed method are summarized as follows:

Step 1: The available data of the target large-scale system, including system parameters and physical structure, should be collected. The steady-state operating points of the system should be calculated accordingly.

Step 2: The impedance/admittance models of all system components (e.g., converters, transmission lines, transformers, loads, shunts) should be derived in dq frame.

Step 3: The targeted system is decomposed into several sub-areas and the corresponding interconnection network, as shown in Fig. 1, where each sub-area contains individual converters and their connection network.

Step 4: The NAM of each sub-area should be derived, and the stability of each sub-area is analyzed using determinant-based GNC with two possible results: 1) all sub-areas are stable; 2) some sub-areas are unstable. For the first possible result, i.e., all sub-areas are identified to be stable, the process can then move to the next step. For the second possible result, i.e., one or more sub-areas are identified to be unstable, and converters that

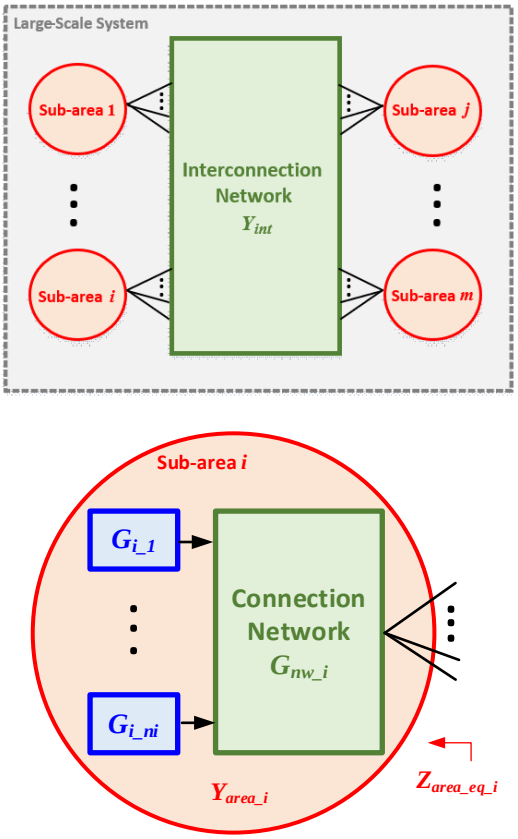

Fig. 1. Area partition of a large-scale power electronics-based power system.

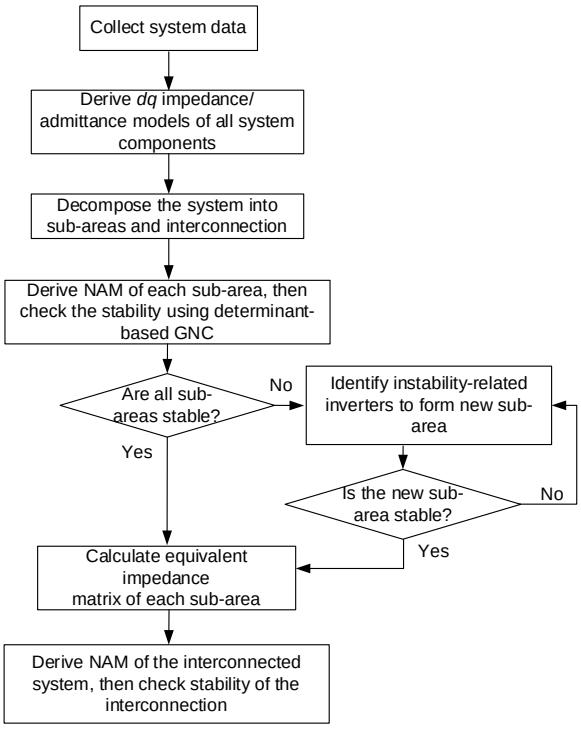

Fig. 2. Flow chart of the NAM-based area partition method.

are related to the instability within the unstable areas can be located using the participation factor (PF) matrix [11]. Then, each instability-related converter will be isolated from the original unstable sub-areas to form a new stable "sub-area" since each converter is designed to be stable. With the newly decomposed single-converter areas, the possible result 2) is updated to be the possible result 1).

Step 5: When all sub-areas are stable, the equivalent impedance matrix of each sub-area seeing from interconnected nodes will be derived. The NAM of the i^{th} sub-area, Y_{area_i}, which includes closed-loop output admittances of all converters within that sub-area, is calculated first. Then, the impedance matrix Z_{area_i} of the sub-area is derived by inverting Y_{area_i} as in (2), where k is the number of buses in that sub-area. With this, the equivalent impedance matrix $Z_{area\_eq\_i}$ can be derived by extracting elements of the columns and rows which correspond to the interconnected nodes. After getting the equivalent impedance matrices of all m sub-areas, the overall equivalent impedance matrix of the interconnected system Z_{area_eq} as in (3).

$$Z_{area\_i} = Y_{area\_i}^{-1} = \begin{bmatrix} Z_{11} & \cdots & Z_{1k} \\ \vdots & \ddots & \vdots \\ Z_{k1} & \cdots & Z_{kk} \end{bmatrix} \quad (2)$$

$$Z_{area\_eq} = \mathrm{diag}[Z_{area\_eq\_1}, Z_{area\_eq\_2}, \cdots, Z_{area\_eq\_m}] \quad (3)$$

Step 6: The admittance matrix of the interconnection network Y_{int} can be derived according to the interconnection structure. Then, the stability of the whole interconnected system can be analyzed using the Nyquist diagrams or the bode plots of $\det(I + Z_{area\_eq} Y_{int})$. If the interconnection is stable, the whole system will be stable. If the interconnection is unstable, the PF matrix can be applied and used to locate the sub-areas (the interconnection nodes) that are related to instability. Note that either in each sub-area or in the interconnection network, buses without connected converters can be eliminated using Kron reduction [12].

The proposed NAM-based area partition method provides several advantages compared to the whole system NAM method. First, it is more scalable and flexible, e.g., when the system topology is reconfigured, only matrices of related sub-areas need to be updated, instead of the large entire system matrix. Second, it provides more stability-related information about the areas and the interconnection lines, i.e., the stability of each control area can be obtained. Third, it helps to save efforts on identifying the weakest point or locating system-instability-related converters using an area-based low-dimension matrix, instead of an entire system-based high-dimension matrix.

III. Case Investigation

A. System Description

To investigate the effectiveness of the proposed NAM-based area partition method, a 6-converter system is adopted as an example case. Fig. 3(a) shows the circuit diagram of the example system, where G_{11}, G_{12}, G_{21}, and G_{22} are four voltage-controlled converters with current feedforward control, while G_{13} and G_{23} are two current-controlled converters with voltage feedforward control. According to the proposed method, the example system is decomposed into 2 sub-areas with an interconnection line first, as shown in Fig. 3(b) under three different cases. In both case I and case II, the interconnection line is connected between bus 11 and bus 21; while in case III, the interconnection line is changed to connect bus 12 and bus 23. Detailed parameters of this 6-converter system are listed in TABLE I.

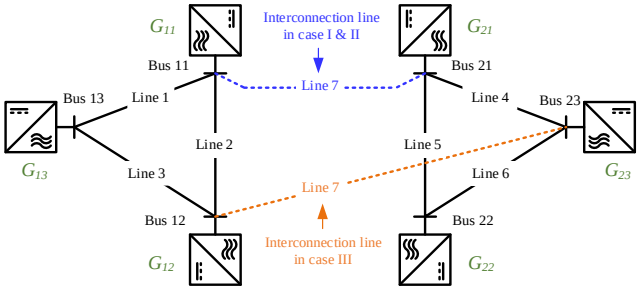

(a)

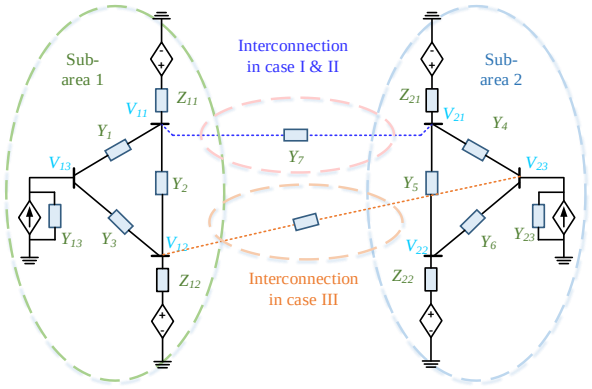

(b)

Fig. 3. (a) the example 6-converter system; (b) area partition of the case I, II, and III

TABLE I. Electrical Parameters of the Six-Converter System

Electrical Parameters		Values
AC voltage base	V_{base}	50 V
AC power base	S_{base}	1302 VA
Fundamental frequency	ω_f	$2\pi \times 60$ rad/s
Line impedances	L_1, R_1	2.45 mH, 0.12 Ω
	L_2, R_2	1.2 mH, 0.04 Ω
	L_3, R_3	0.7 mH, 0.035 Ω
	L_4, R_4	10.7 mH, 0.65 Ω
	L_5, R_5	2.5 mH, 0.12 Ω
	L_6, R_6	0.7 mH, 0.04 Ω
	L_7, R_7	0.7 mH, 0.035 Ω

TABLE II. PARAMETERS OF CONVERTERS

Electrical Parameters		Values
L filter	L_f, R_f	0.575 mH, 0.2 Ω
DC voltage	V_{dc}	200 V
Switching frequency	f_{sw}	10 kHz
Voltage-Controlled Converters		**Values**
PI voltage controller	K_{vp}, K_{vi}	1.04, 325
Voltage measurement filter	ω_{fv}	$2\pi \times 300$ rad/s
Current measurement filter	ω_{fc}	$2\pi \times 1000$ rad/s
Current-Controlled Converters		**Values**
PLL PI parameters	K_{pllp}, K_{plli}	1.06, 18
PI current controller	K_{ip}, K_{ii}	2.6, 2275
Voltage feed-forward gain	ω_{ffv}	$2\pi \times 200$ rad/s

B. Impedance/admittance models of system components

To analyze the example scale-down system, the dq impedance models of all system components, including transmission lines, voltage-controlled converters, and current-controlled converters, need to be derived first. The dq impedance and admittance of each transmission line can be modeled as:

$$Z_{TL} = \begin{bmatrix} R + sL & -\omega_f L \\ \omega_f L & R + sL \end{bmatrix}, Y_{TL} = Z_{TL}^{-1} \tag{4}$$

where R and L are the resistance and the inductance of each transmission line, respectively.

The dq impedance and admittance of voltage-controlled and current-controlled converters can be modeled as follows [13]. For the voltage-controlled converters, the dq output impedance model is:

$$\begin{aligned} Z_{ov} = T_\theta^{-1}\left(I + G_{vo}G_dG_vG_{fv}G_{sv}\right)^{-1} \times \\ \left[Z_o - G_{vo}G_d\left(G_{ffc}G_{fc} + G_{vdec}\right)G_{sc}\right]T_\theta \end{aligned} \tag{5}$$

where T_θ is the transformation matrix between two dq frames; Z_o and G_{vo} represents the output filter; G_v represents the voltage PI controller; G_d represents the delay component; G_{vdec} is the decoupling term; G_{sv} and G_{sc} are transfer function matrices for voltage and current measurement; G_{fv}, G_{fc}, and G_{ffc} are the voltage filter, current filter, and current feed-forward gain, respectively.

For the current-controlled converters, the dq output admittance model is:

$$\begin{aligned} Y_{oc} = [I + Y_oG_dT_\theta^{-1}(G_c - G_{cdec})T_\theta G_{sc}]^{-1}Y_o \times \\ \left\{I - G_dT_\theta^{-1}\left[G_{ffv}G_{vt} - (G_c - G_{cdec})G_i - G_{vc}\right]T_\theta G_{sv}\right\} \end{aligned} \tag{6}$$

where Y_o is the admittance matrix of the output filter; G_c represents the current PI controller; G_{cdec} is the decoupling term; G_{ffv} is the voltage feed-forward gain; G_{vt}, G_i, and G_{vc} represent the PLL impact. Definitions of T_θ, G_d, G_{sc}, and G_{sv} are the same as in (5).

C. Analytical results

To verify the proposed method, three different cases of the example system are analyzed. In case I, the system is stable with a reference design shown in TABLE I and TABLE II. In both case II and III, the cutoff frequency of voltage feedforward control of G_{23} is increased from $2\pi \times 200$ rad/s to $2\pi \times 1000$ rad/s. Also, the interconnection Line 7 is changed to connect Bus 12 and Bus 23 in case III. Fig. 4 shows the Bode diagrams of analysis results for the six-converter system using the proposed method. When analyzing the stability of the system, the Bode diagram is a better way considering the large magnitude variation in the Nyquist diagram, and 180° decrease of phase angle in the Bode diagram represents that the origin point $(0, j0)$ is encircled once in the clockwise direction [9].

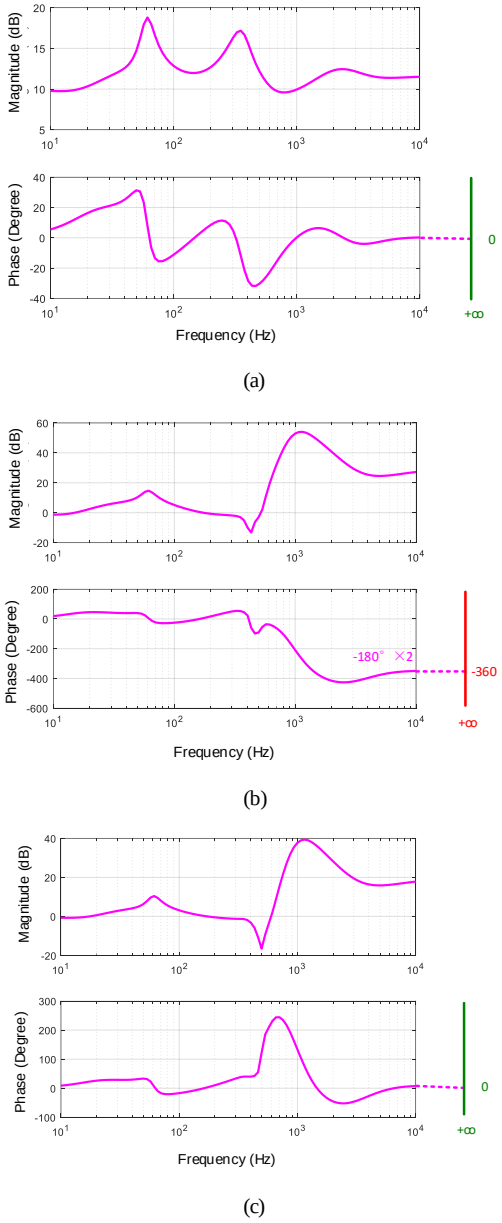

Fig. 4. Bode plots of the interconnected system: (a) case I; (b) case II; (c) case III.

In case I, both sub-area 1 and sub-area 2 are determined to be stable, and the interconnection of the two sub-areas is also predicted to be stable, as shown in Fig. 4(a), where the phase variation in the full positive frequency range is 0°.

In case II, the sub-area 1 is determined to be stable, but the sub-area 2 is found to be unstable. Then, the absolute values of the PF matrix are calculated for sub-area 2 in TABLE III. Note that only the eigenvalues that encircle the critical point should be considered, which is λ_3 in this case, and the PF values are calculated at the unstable frequency. Larger PF values mean the corresponding converters are more relevant to the corresponding eigenvalues. As shown in Table III, G_{23} is identified as the system-instability-related converter. As explained in Fig. 2, G_{23} will form a new sub-area, while G_{21} and G_{22} will form another new sub-area. The Bode diagrams of the interconnection of all these areas are shown in Fig. 4(b). The overall system is found to be unstable in this case, since the phase variation is $-180^{\circ} \times 2 = -360^{\circ}$, which means there are 2 RHP poles in case II.

TABLE III. ABSOLUTE VALUES OF PARTICIPATION FACTORS IN CASE II

Converters	λ_3
G_{21}	0.0361
	0.0398
G_{22}	0.0770
	0.0856
G_{23}	**0.3283**
	0.3641

In case III, similar processes are done as in case II when analyzing the stability of the two sub-areas, and the system is predicted to be stable with the changed interconnection line compared to case II, as shown in Fig. 4(c), where the phase variation is 0°.

IV. SIMULATION AND EXPERIMENTAL VERIFICATION

To verify the results of the proposed small-signal analysis method, both the simulation model and the experimental platform of the example system are established. The same parameters in TABLE I and TABLE II are used in both simulations and experiments.

A. Simulation Results

A six-converter system with the same parameters in TABLE I and TABLE II is established in MATLAB/Simulink. Fig. 5 shows the simulation results of the three corresponding cases as described in Section III. It can be found that the analytical results obtained by the proposed method match well with the simulation waveforms, where case I and III are stable, and case II is unstable.

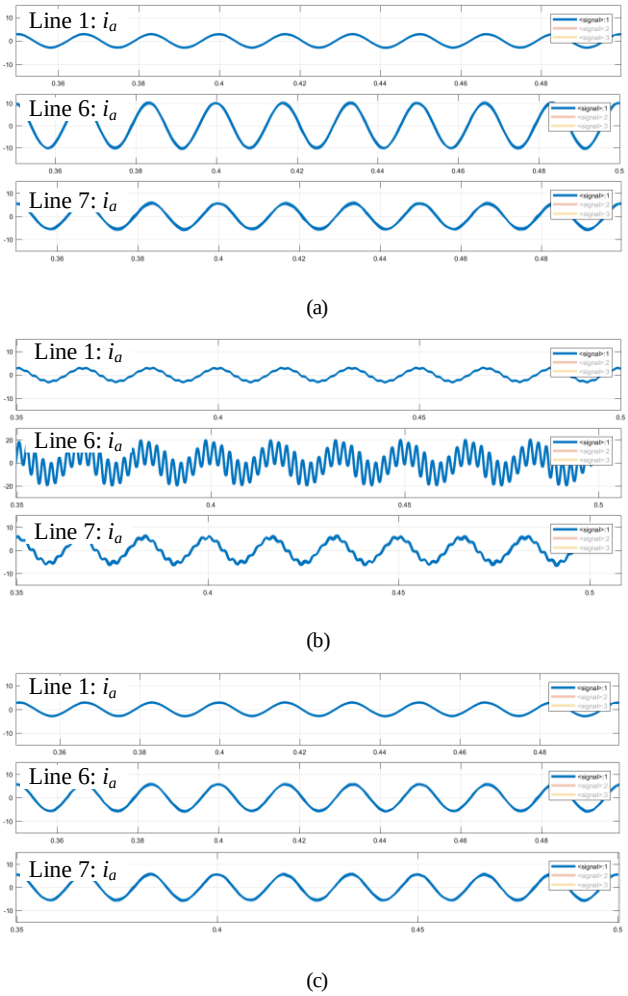

Fig. 5. Simulation waveforms of (a) case I; (b) case II; (c) case III.

B. Experimental results

The experimental platform is built based on the hardware testbed (HTB) to simulate the six-converter system, as shown in Fig. 6 [14, 15]. The converter cabinet in Fig. 6(a) contains the six converters used in the example system, while the variable inductor cabinet in Fig. 6(b) is used to emulate the impedance of the system transmission lines.

(a) (b)

Fig. 6. HTB setup: (a) converter cabinet, (b) variable inductor cabinet.

Fig. 7 shows the experimental waveforms in the three cases as described in Section III, where both case I and case III are stable, while case II is unstable. Hence, it can be concluded that the experimental results match the analytical results in section III-C.

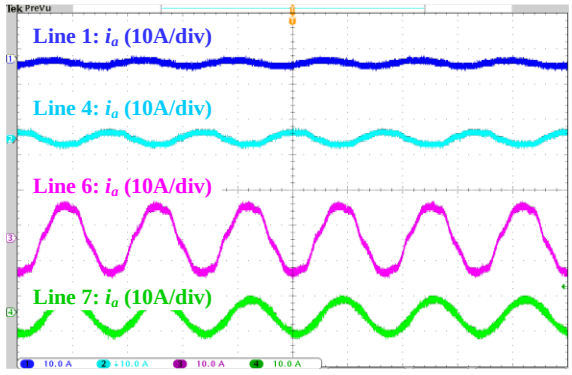

(a)

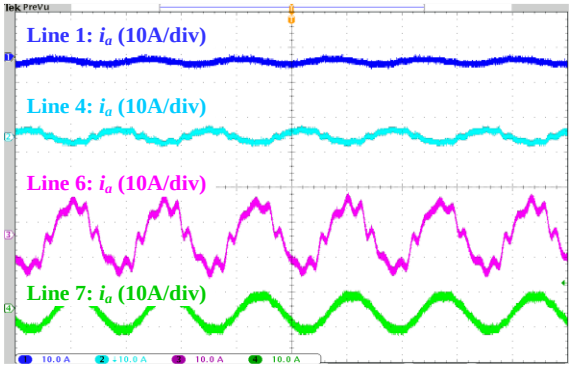

(b)

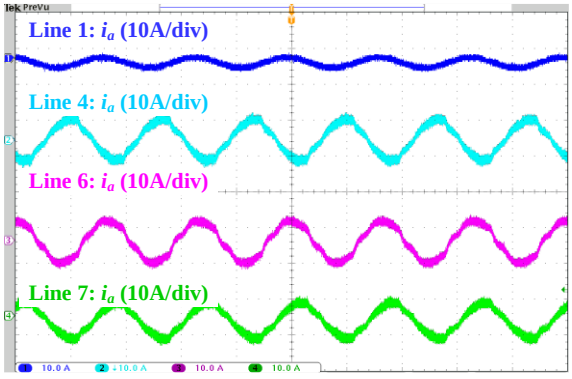

(c)

Fig. 7. Experimental waveforms of the example system: (a) case I; (b) case II; (c) case III.

V. Conclusions and Future Work

This paper proposes a NAM-based area partition method to analyze the small-signal stability of large-scale PEPSs. The whole system is decomposed into several sub-areas, and the stability within each sub-area is analyzed first. Then, the small-signal stability of the overall system is analyzed using the determinant-based GNC for the interconnection of all sub-areas. A six-converter system is used as an example system to demonstrate the proposed method in both simulation and experiment. Compared with the whole system NAM method, the proposed method shows improved flexibility and scalability under system contingency. It also provides more stability-related information and can help to locate the system's weak points. The future work includes the performance verification of the proposed method using larger PEPSs.

Notice of Copyright

Acknowledgment

This material is based upon work supported by the US Department of Energy, Office of Electricity, Advanced Grid Modeling Program under contract DE-AC05-00OR22725. This work is primarily supported by Oak Ridge National Lab. This work also made use of Engineering Research Center Shared Facilities provided by the Engineering Research Center Program of the National Science Foundation and the Department of Energy under NSF Award Number EEC1041877 and the CURENT Industry Partnership Program.

References

[1] J. M. Guerrero, F. Blaabjerg, T. Zhelev, K. Hemmes, E. Monmasson, S. Jemei, M. P. Comech, R. Granadino, and J. I. Frau, "Distributed generation: Toward a new energy paradigm," *IEEE Industrial Electronics Magazine*, vol. 4, no. 1, pp. 52-64, 2010.

[2] N. G. Hingorani, "Power electronics in electric utilities: role of power electronics in future power systems," *Proceedings of the IEEE*, vol. 76, no. 4, pp. 481-482, 1988.

[3] L. Kristov, "The bottom-up (R) Evolution of the electric power system: The pathway to the integrated-decentralized system," *IEEE Power and Energy Magazine*, vol. 17, no. 2, pp. 42-49, 2019.

[4] X. Wang and F. Blaabjerg, "Harmonic Stability in Power Electronic-Based Power Systems: Concept, Modeling, and Analysis," *IEEE Transactions on Smart Grid*, vol. 10, no. 3, pp. 2858-2870, 2019.

[5] M. Amin and M. Molinas, "Small-Signal Stability Assessment of Power Electronics Based Power Systems: A Discussion of Impedance- and Eigenvalue-Based Methods," *IEEE Transactions on Industry Applications*, vol. 53, no. 5, pp. 5014-5030, 2017.

[6] C. Zhang, M. Molinas, A. Rygg, and X. Cai, "Impedance-based analysis of interconnected power electronics systems: Impedance network modeling and comparative studies of stability criteria," *IEEE Journal of Emerging and Selected Topics in Power Electronics*, 2019.

[7] X. Wang, F. Blaabjerg, and W. Wu, "Modeling and Analysis of Harmonic Stability in an AC Power-Electronics-Based Power System," *IEEE Transactions on Power Electronics*, vol. 29, no. 12, pp. 6421-6432, 2014.

[8] W. Zhou, R. E. Torres-Olguin, Y. Wang, and Z. Chen, "A Gray-Box Hierarchical Oscillatory Instability Source Identification Method of Multiple-Inverter-Fed Power Systems," *IEEE Journal of Emerging and Selected Topics in Power Electronics*, pp. 1-1, 2020.

[9] W. Cao, Y. Ma, L. Yang, F. Wang, and L. M. Tolbert, "D–Q Impedance Based Stability Analysis and Parameter Design of Three-Phase Inverter-Based AC Power Systems," *IEEE Transactions on Industrial Electronics*, vol. 64, no. 7, pp. 6017-6028, 2017.

[10] Y. Li, Z. Shuai, X. Liu, Y. Chen, Z. Li, Y. Hong, and Z. J. Shen, "Stability Analysis and Location Optimization Method for Multi-converter Power Systems Based on Nodal Admittance Matrix," *IEEE Journal of Emerging and Selected Topics in Power Electronics*, 2019.

[11] X. Wilsun, H. Zhenyu, C. Yu, and W. Haizhen, "Harmonic resonance mode analysis," in *IEEE Power Engineering Society General Meeting, 2005*, 16-16 June 2005 2005, p. 2236 Vol. 3.

[12] L. Luo and S. V. Dhople, "Spatiotemporal model reduction of inverter-based islanded microgrids," *IEEE Transactions on Energy Conversion*, vol. 29, no. 4, pp. 823-832, 2014.

[13] W. Cao, "Impedance-based stability analysis and controller design of three-phase inverter-based ac systems," 2017.

[14] L. Yang, Y. Ma, J. Wang, J. Wang, X. Zhang, L. M. Tolbert, F. Wang, and K. Tomsovic, "Development of converter based reconfigurable power grid emulator," in *2014 IEEE Energy Conversion Congress and Exposition (ECCE)*, 14-18 Sept. 2014 2014, pp. 3990-3997.

[15] J. Wang, L. Yang, Y. Ma, J. Wang, L. M. Tolbert, F. Wang, and K. Tomsovic, "Static and dynamic power system load emulation in a converter-based reconfigurable power grid emulator," *IEEE Transactions on Power Electronics*, vol. 31, no. 4, pp. 3239-3251, 2016.